

Double-core excitations in formamide can be probed by X-ray double-quantum-coherence spectroscopy

Yu Zhang, Daniel Healion, Jason D. Biggs, and Shaul Mukamel

Citation: *J. Chem. Phys.* **138**, 144301 (2013); doi: 10.1063/1.4798635

View online: <http://dx.doi.org/10.1063/1.4798635>

View Table of Contents: <http://jcp.aip.org/resource/1/JCPSA6/v138/i14>

Published by the [American Institute of Physics](#).

Additional information on *J. Chem. Phys.*

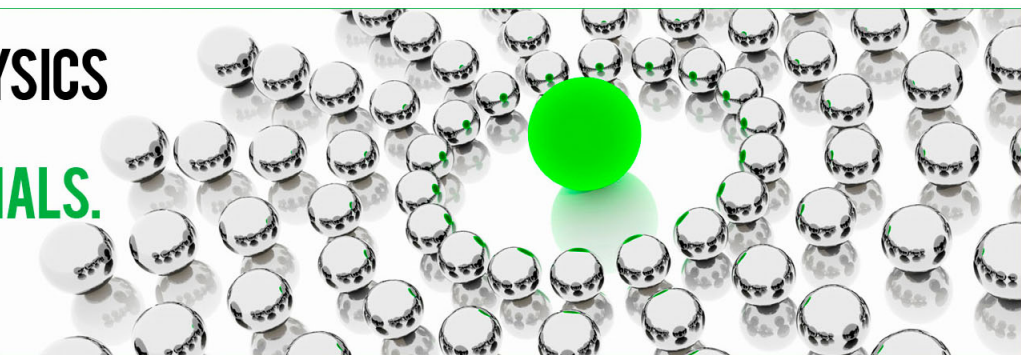
Journal Homepage: <http://jcp.aip.org/>

Journal Information: http://jcp.aip.org/about/about_the_journal

Top downloads: http://jcp.aip.org/features/most_downloaded

Information for Authors: <http://jcp.aip.org/authors>

ADVERTISEMENT



**ALL THE PHYSICS
OUTSIDE OF
YOUR JOURNALS.**

physics
today

www.physics today.org

Double-core excitations in formamide can be probed by X-ray double-quantum-coherence spectroscopy

Yu Zhang, Daniel Healion, Jason D. Biggs, and Shaul Mukamel^{a)}

Department of Chemistry, University of California, 450 Rowland Hall, Irvine, California 92697, USA

(Received 24 January 2013; accepted 12 March 2013; published online 10 April 2013)

The attosecond, time-resolved X-ray double-quantum-coherence four-wave mixing signals of formamide at the nitrogen and oxygen K-edges are simulated using restricted excitation window time-dependent density functional theory and the excited core hole approximation. These signals, induced by core exciton coupling, are particularly sensitive to the level of treatment of electron correlation, thus providing direct experimental signatures of electron and core-hole many-body effects and a test of electronic structure theories. © 2013 American Institute of Physics. [<http://dx.doi.org/10.1063/1.4798635>]

I. INTRODUCTION

New attosecond X-ray table top sources^{1,2} and X-ray free electron lasers (XFEL)^{3,4} will extend nonlinear spectroscopic techniques, originally developed to study valence excitonic systems, to molecular core excitations. XFEL sources are bright enough to saturate the core-excitation transitions,^{5,6} and should enable fundamental questions about the quasiparticle description of many-electron states to be experimentally addressed. Nonlinear techniques designed to probe quantum correlations in systems at lower energies with slower dynamics may thus be extended to the X-ray frequency regime. The core electrons are tightly bound to specific atoms and are strongly coupled to a slower bath of correlated valence electrons shared between atoms. 1D- and 2D-stimulated X-ray Raman techniques have been proposed to examine valence electron dynamics using core holes as ultrafast switches.

This paper focuses on doubly core-excited states (DCESs), in which the main players are the static core holes and the virtual orbitals. These states correspond to the high-energy limit of double valence excitations, which are challenging to treat with density functional theory (DFT) methods.⁷ Multiply excited states can be prepared by short and intense laser pulses.⁸ It has been suggested that DCESs carry information about the chemical environment of a selected atom in double photoionization core-excitation spectroscopy.^{9–11} Recent experimental^{12,13} and theoretical^{9,11} work demonstrated a static frequency shift of doubly-core-photoionized states that depends on their local chemical environment. The double-quantum-coherence (DQC) signal¹⁴ preferentially targets doubly excited states in an excitonic system.¹⁵ This signal strongly depends on the coupling between excitons; infrared DQC signals, which have been used to study vibrational couplings in the amide I band,¹⁶ sensitively depend on anharmonicities, vanishing for harmonic vibrational systems. In the visible, DQC has been used to investigate the excitations of a dye molecule in ethanol,¹⁷ and

theoretical studies have demonstrated a strong dependence on electron correlations in model two and three-level semiconductor systems.¹⁸ DQC can monitor the breakdown of mean-field theories of electron correlation in molecular systems. This technique has also been applied to measure spin selected biexciton coupling using circularly polarized pulses,^{19,20} and interatomic couplings in a dilute potassium vapor.²¹ The X-ray version of this technique (XDQC) is sensitive to correlation and exciton scattering in DCESs, making it an attractive experimental test for many-body electron structure techniques for strongly correlated systems.^{22–24} XDQC detects only systems in which the single core excitations affect each other and the doubly core-excited wavefunction may not be factorized into an outer product of two singly core-excited wavefunctions. For uncoupled core excitations, two contributions to the signal (see Sec. IV) with opposite signs cancel out and the signal vanishes. Incomplete cancellation therefore provides a sensitive measure of correlation between core excitations.

Core-excited states can be calculated at various levels of theory. The XDQC signal was first simulated for all nitrogen excitations of isomers of aminophenol with a simple equivalent core approximation (ECA), which describes the effect of the core hole on the valence excited states.²⁵ In this study we employ restricted excitation window time-dependent density functional theory (REW-TDDFT),^{26–32} a response formalism that incorporates the core-hole-valence coupling through an exchange-correlation functional. This approach was recently used to calculate the single core excitations and stimulated X-ray Raman signal of cysteine.³³

Here we simulate the XDQC signals of formamide, a small organic molecule containing carbon, nitrogen, and oxygen, which is often used as a model for the peptide backbone in proteins (see Fig. 3). Its X-ray spectra has been investigated both experimentally^{34–36} and theoretically.³⁷ Formamide has been used as a benchmark in theoretical studies of double core hole spectroscopy^{38,39} and in molecular dynamics⁴⁰ and vibrational spectroscopy applications.^{41,42}

We summarize the theoretical methods and computational challenges of double excitations in Sec. II. Our treatment of core and valence excited states is presented in

^{a)}smukamel@uci.edu

Sec. III. Sum over states expressions for XDQC signals involving the core-excited eigenstate frequencies and transition dipole matrix elements are given in Sec. IV. We then apply the REW-TDDFT to calculate the orientationally averaged X-ray absorption near edge structure (XANES) and XDQC signals of formamide at the N and O K-edges. The results are discussed in Sec. VI.

II. ELECTRONIC STRUCTURE SIMULATIONS OF DOUBLE EXCITATIONS

Electronic excited states can often be represented as linear combinations of single excitations, where a single electron is promoted from an occupied to a virtual orbital. Some of the most popular and inexpensive computational methods for excited states, such as configuration interaction singles (CIS) and TDDFT, are based on this picture. While often adequate for molecules or high bandgap materials they fail badly for double excitations in conjugated or metallic systems with strong valence band correlations. Double-exciton states, which are common in molecular crystals⁴³ and materials with strong spatial localization,⁴⁴ also play a role in conical intersections, long-range charge-transfer excitations and autoionizing resonances.⁷ Low-lying excited states in polyenes with significant double-excitation character are notable examples in which the single excitation picture fails qualitatively to describe the system.^{45–52} Strong double-excitation features in XANES spectroscopy have been reported for ferrocene and ferrocenium compounds,⁵³ and it has been shown that double or higher-order excited configurations are necessary to construct the spin-symmetry-adapted wavefunctions of molecules with open-shell ground states.^{54–57}

Formally any state with energy close to the sum of two single excitation energies can be considered a double excitation. However this may not be always justified. The doubly excited states in polyenes mentioned above are examples where this assignment completely breaks down, since they are lower in energy than any single excited state.⁴⁸ To define double excitations, we must first specify the reference single-particle theory and define the orbitals and their energies. In some cases a Hartree-Fock ground state reference suggests a significant double-excitation character for an excited state while a Kohn-Sham ground state reference does not.^{7,55} Various high-level *ab initio* methods also show very different double-excitation character,^{48,58} since DCESs are directly related to correlation. The XDQC technique creates DCESs by using two pulses. In contrast with valence shake-up excitations in XANES induced by the core-hole Coulomb interaction, in two photon core excitation each core is prepared by a different photon. In this paper we consider the valence relaxation in the field of the first core hole explicitly, and neglect any accompanying Auger, nuclear, or electronic processes within the very short duration of the measurement.

High-level *ab initio* techniques are usually required to handle double excitations in the valence band.⁵⁹ These include complete active space self-consistent field (CASSCF), complete active space perturbation theory of second order (CASPT2),⁵¹ coupled cluster (CC),⁶⁰ multireference con-

figuration interaction (MRCI),^{52,61} symmetry-adapted cluster configuration interaction (SAC-CI),⁶² algebraic diagrammatic construction (ADC),^{48–50} and multireference Møller-Plesset perturbation theory (MRMP).^{46,58} These accurate techniques are computationally expensive and limited to small molecular systems such as polyenes with several carbon atoms.

TDDFT^{63,64} balances accuracy and computational cost for excited states. Most implementations invoke the adiabatic approximation, by assuming that the exchange-correlation (XC) kernel, the second functional derivative of the XC energy with respect to density, is frequency independent. Maitra *et al.*⁶⁵ showed that a frequency-dependent XC kernel is necessary to correctly describe a state with a strong double-excitation mixing. Double-excitation energies using the adiabatic form of the quadratic response are simply the sums of two single excitation energies,^{7,66,67} unlike early claims to the contrary.⁶⁸ These trivial double-excitation energies may not be found within the Tamm-Dancoff approximation.⁶⁹ Maitra *et al.*⁶⁵ also proposed dressed TDDFT to remedy this deficiency; deriving a frequency-dependent XC kernel in which single excitations are mixed with spectrally isolated double excitations. This approach has been applied and tested.^{70–73} Its major weakness is the need to assign the mixed single and double excitations *a priori*.

Many additional density functional methods have been proposed for doubly-excited systems. Casida had added non-DFT many-body polarization propagator correction based on the Bethe-Salpeter equation to the XC kernel.⁵⁴ This non-adiabatic XC kernel includes the dressed TDDFT kernel as a special case if the ground state has a closed shell. Additional frequency-dependent XC kernels accounting for double excitations in finite and correlated systems were derived recently from the Bethe-Salpeter equation.^{44,74} The spin-flip (SF) approach^{75–79} is also a promising method for generating double excited states from a triplet single-reference state, in which electrons are excited to an orbital with a different spin. The SF approach can be employed to both wavefunction-^{75–78} and TDDFT⁷⁹ based methods. In the original implementation of SF-TDDFT, the coupling of SF excitations entered the linear response equation only through the Hartree-Fock exchange component in the hybrid XC functionals. Wang and Ziegler overcame this limitation by a noncollinear formulation of the XC potential.⁸⁰ Recent assessment and applications of SF-TDDFT are given in Refs. 81–84. The real-time approach has also been used to obtain double excitations.^{85,86} A time-independent DFT method for multiple excitations was proposed recently.^{87,88} In this approach multiply-excited states were obtained from an optimized effective potential (OEP) eigenvalue equation with orthogonality constraints. Computing the OEP of a polyatomic molecule, however, is not easy, and there are still many open questions in the DFT response formalism for excited states. Time-dependent density matrix functional theory (TDDMFT), proposed by Giesbertz *et al.*,⁸⁹ may also account for double excitations. Adopting these methods to better describe the processes that contribute to various nonlinear spectroscopy techniques, and designing experiments which test the assumptions underlying them, is an ongoing open challenge.

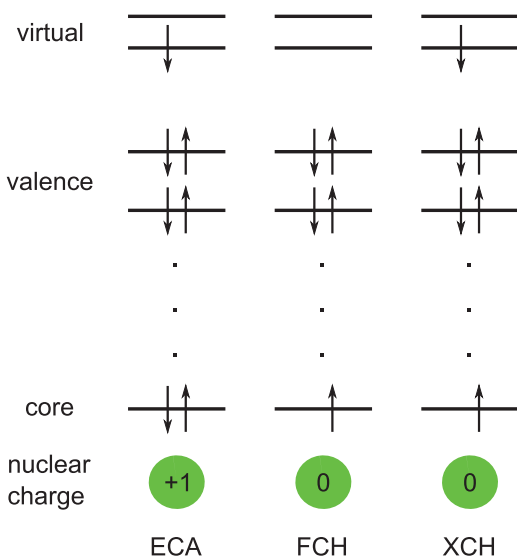


FIG. 1. Schematics of self-consistent calculation of core-excited states. The ECA (left) replaces a core with the next highest element in the periodic table, the FCH (middle) fixes the occupation of the core-orbital, neglecting the excited electron, whereas the XCH (right) fixes the occupation of both orbitals.

III. THEORY

A. Survey of approximations for single core holes

The three most common approximate descriptions of core excitations are illustrated in Fig. 1. The ECA, also known as the $Z + 1$ approximation,^{90,91} replaces the core hole by an additional nuclear charge, and was employed in our previous simulation studies of X-ray nonlinear spectroscopy signals.^{25,92–95} The ECA can be easily implemented within the routine features of standard quantum chemistry packages, and easily represents DCESs using two extra nuclear charges. However, it is only applicable to deep core holes as it neglects the effect of the chemical environment, changes the spin symmetry of a single core-hole state,⁹⁶ and cannot account for core-hole delocalization and migration.

The full core hole (FCH) approximation⁹⁷ improves on the basic ECA model by employing orbitals determined self-consistently using the fixed core-hole configuration as shown in the middle panel of Fig. 1. The direct static exchange (STEX) model^{98,99} is one type of FCH with the occupied Hartree-Fock orbitals and the improved virtual orbitals (IVO)¹⁰⁰ of the ionic ($N - 1$)-electron system. Unlike the ECA, STEX includes orbital relaxation and can be applied to both deep and shallow core holes. Interactions between the excited electron and the other $N - 1$ inner electrons, however, are still neglected. We have used STEX to study linear and nonlinear X-ray spectroscopy signals^{33,101,102} in small organic molecules. A detailed analysis of STEX and comparison with REW-TDDFT is given in Refs. 101 and 33. Current implementations of STEX are limited to single core-hole states. Spin coupling of the two core electrons complicates the DCES wavefunction, making it hard to map to an effective single-particle Hamiltonian like that in STEX. Self-consistent field (SCF) calculations of DCESs are also numerically tricky, and frequently fail to converge. Previous calculations of double core-hole states using CASSCF,^{13,39,103} MRCI,^{11,104} and

ADC^{9,11,105,106} are expensive and had only been applied to small molecules such as NH_3 and CH_4 . Relativistic corrections may be necessary for core electrons.^{11,107} The much cheaper Δ SCF methods,^{11,107–109} such as STEX, suffer from SCF convergence problems for core-hole states.¹¹⁰ Moreover, running many SCF calculations with combinations of core-holes and excited electrons is tedious.

We employ a third approach, REW-TDDFT, first proposed by Stener *et al.* in 2003²⁶ and further developed in additional studies.^{27,28} REW-TDDFT only considers electrons excited from a defined set of relevant orbitals (the restricted excitation window), allowing to obtain high-lying states in the excitation spectrum without calculating the lower states. A similar restricted channel approach was suggested in Ref. 111, without orbital relaxation in the field of the core hole. Like TDDFT, the complex polarization propagator method¹¹¹ is also based on response theory. With this method, the absorption of the system at a given frequency can be calculated by solving a response matrix equation; the interesting energy region can be sampled without solving explicitly for the excited states. This method was applied in Ref. 112.

We have recently found³³ REW-TDDFT to be more accurate in predicting frequency splitting in XANES and computationally less demanding than STEX. Brena *et al.* had pointed out that TDDFT core-excitation energies have larger absolute errors than those from STEX or transition-state calculations, because TDDFT does not account for orbital relaxation and self-interaction of core electrons.¹¹³ We found the same trend.³³ Apart from an overall shift, TDDFT core excitation energies agree with the XANES of many systems very well.^{31,32,114} The TDDFT core-edge energy can be improved by applying the Perdew-Zunger self-interaction correction scheme,^{115,116} or by employing recently-developed core-valence hybrid functional,^{117–119} long-range corrected hybrid functional with short-range Gaussian attenuation¹²⁰ and short-range corrected functionals.^{29,30} These techniques yield core-edge energies with errors less than 1 eV on a series of small molecules.^{29,30} More precise benchmarks will be needed to compare the accuracy of STEX and REW-TDDFT.

B. Double-core excitations

Adiabatic TDDFT cannot deal with double excitations.⁶⁵ Practical frequency-dependent XC kernels for medium or large molecular systems have yet to be developed. Both TDDFT and the excited state core hole (XCH) method¹²¹ treat singly core-excited state (SCES) very well. The excited electron in XCH approximation is included self-consistently through a full core-hole state. XCH has been applied to solid state X-ray absorption spectra with pseudopotentials, and applying it to molecular system poses no additional difficulty. We will use XCH in this paper. Pseudopotentials can be constructed for single¹²² and double core-hole states. An effective potential which ignores the polarizability of the core hole in different chemical environments will introduce errors into practical calculations. A fixed pseudopotential of a core hole, like the ECA, ignores all core-hole dynamics.

Here we employ an approach that combines XCH and REW-TDDFT. We first run an SCF calculation to get a reference state SCES0, with a core hole and an excited electron. This reference is then used to run a REW-TDDFT calculation to obtain excited states with two core holes and two excited electrons. Adiabatic TDDFT only treats single excitations of the SCES0 reference, not all double core excited states are accounted for. Additional DCESs can be found by starting REW-TDDFT at different SCES references, obtained by permuting the occupied and virtual orbitals of SCES0 (orbital approximation as in Ref. 101).

Unrestricted reference-based TDDFT is known to suffer from spin contamination.^{55,123} A truncated rank of excitations from one component of a spin multiplet generates an incomplete configuration space for the total spin operator \hat{S}^2 .^{57,124,125} Stated differently, higher rank excited configurations are needed to represent a pure spin state. Our current TDDFT calculations on a spin symmetry-broken reference state are no exception, but since the singlet-triplet energy splitting is negligible compared to the large energies of core excitations, spin contamination does not strongly affect the calculated core-excitation energies. Casida and co-workers suggested to use the difference of the total spin between excited states and the reference state ($\Delta\langle S^2 \rangle$) in order to filter out unphysical excited states.¹²³ We follow his scheme by only including excited states with small $\Delta\langle S^2 \rangle$ s in our calculations.

The two sequential core excitations cannot be treated in the same fashion. After the initial excitation, the valence electrons relax self-consistently (XCH) in the field of the core hole, and the second excitation is treated using response theory (REW-TDDFT). This treatment uses two potentials to perturb the valence band during the second excitation: a strong, long duration core-hole potential which must be

treated nonperturbatively, and the ultrafast second photon excitation, which can be truncated at first order using response theory. This physically intuitive order in which relaxation precedes photon excitation strongly effects the signal, as we show later by reversing it, treating the original first core excitation using REW-TDDFT and the original second using XCH.

IV. THE DQC SIGNAL

The DQC signal employs four pulses with wave vectors satisfying $\mathbf{k}_{\text{III}} = \mathbf{k}_1 + \mathbf{k}_2 - \mathbf{k}_3$, and the transmission change of the \mathbf{k}_{III} pulse is recorded versus the three interpulse delays (t_1, t_2, t_3) (as shown in Fig. 2). The applied electric field is

$$E(t) = \sum_{j=1,2,3,4} E_j(t - \bar{\tau}_j) + \text{c.c.} \quad (1)$$

We represent the pulses as

$$E_j(\mathbf{r}, t - \bar{\tau}_j) = \varepsilon_j(t - \bar{\tau}_j) \exp[i\mathbf{k}_j \cdot \mathbf{r} - i\omega_j(t - \bar{\tau}_j)] \quad (2)$$

with central frequencies ω_j , wave vectors \mathbf{k}_j ($\mathbf{k}_4 = \mathbf{k}_{\text{III}}$), and Gaussian envelopes

$$\varepsilon_j(t - \bar{\tau}_j) = \frac{E_j^0 \exp[-(t - \bar{\tau}_j)^2/2\sigma_j^2]}{\sigma_j \sqrt{2\pi}} \quad (3)$$

with amplitudes E_j^0 , temporal widths σ_j and envelope centers $\bar{\tau}_j$. The XDQC signal depends on the three (positive) delay times ($t_j = \bar{\tau}_{j+1} - \bar{\tau}_j$) or their Fourier conjugates ($\Omega_1, \Omega_2, \Omega_3$). Invoking the rotating wave approximation and assuming temporally well-separated pulses,¹²⁶ the signal is given by the two loop diagrams of Fig. 3,^{127,128}

$$S_{\text{III}}(\Omega_3, \Omega_2, \Omega_1) = S_{\text{III:A}}(\Omega_3, \Omega_2, \Omega_1) + S_{\text{III:B}}(\Omega_3, \Omega_2, \Omega_1), \quad (4)$$

where

$$S_{\text{III:A}}^{v_4 v_3 v_2 v_1}(\Omega_3, \Omega_2, \Omega_1) = \sum_{f'e'} \frac{(\mu_{ge'}^{v_4} \varepsilon_4^*(\omega_4 - \omega_{e'g})) (\mu_{e'f}^{v_3} \varepsilon_3^*(\omega_3 - \omega_{fe'})) (\mu_{fe}^{v_2} \varepsilon_2(\omega_2 - \omega_{fe})) (\mu_{eg}^{v_1} \varepsilon_1(\omega_1 - \omega_{eg}))}{(\Omega_3 - \omega_{e'g} + i\gamma_{e'g})(\Omega_2 - \omega_{fg} + i\gamma_{fg})(\Omega_1 - \omega_{eg} + i\gamma_{eg})} \quad (5)$$

and

$$S_{\text{III:B}}^{v_4 v_3 v_2 v_1}(\Omega_3, \Omega_2, \Omega_1) = - \sum_{f'e'} \frac{(\mu_{e'f}^{v_4} \varepsilon_4^*(\omega_4 - \omega_{fe'})) (\mu_{ge'}^{v_3} \varepsilon_3^*(\omega_3 - \omega_{e'g})) (\mu_{fe}^{v_2} \varepsilon_2(\omega_2 - \omega_{fe})) (\mu_{eg}^{v_1} \varepsilon_1(\omega_1 - \omega_{eg}))}{(\Omega_3 - \omega_{fe'} + i\gamma_{fe'}) (\Omega_2 - \omega_{fg} + i\gamma_{fg}) (\Omega_1 - \omega_{eg} + i\gamma_{eg})}. \quad (6)$$

Here, $\varepsilon_j(\omega)$ is the spectral envelope of the j th pulse (given by the Fourier transform of Eq. (3)), $v_{1\dots 4}$ are the tensor components of the transition dipole μ_{rs} , ω_{rs} is the transition frequency between the states r and s , and γ_{rs} is phenomenological parameter describing the inverse lifetime of the core excited state. Different experimental techniques measure various projections of the full three-dimensional response in Eq. (4). Since XDQC resonances show up along Ω_2 we shall display two 2D projections of this 3D signal

$$S_{\text{III}}(t_3, \Omega_2, \Omega_1) = \int_{-\infty}^{\infty} e^{-i\Omega_3 t_3} S_{\text{III}}(\Omega_3, \Omega_2, \Omega_1) d\Omega_3, \quad (7)$$

where we hold t_3 fixed, and

$$S_{\text{III}}(\Omega_3, \Omega_2, t_1) = \int_{-\infty}^{\infty} e^{-i\Omega_1 t_1} S_{\text{III}}(\Omega_3, \Omega_2, \Omega_1) d\Omega_1 \quad (8)$$

for a fixed t_1 . Fixed, nonzero $t_{1,3}$ avoid the possibility of overlapping pulses contributing to the signal. There are three independent tensor components of the signal in isotropic media which depend on contractions over different field polarization vectors. The signal in an isotropic sample is a linear combination of various contractions over the tensor components $v_{1\dots 4}$ in Eq. (4). The rotationally averaged signal with all parallel pulse polarizations is given by Eq. (A5).

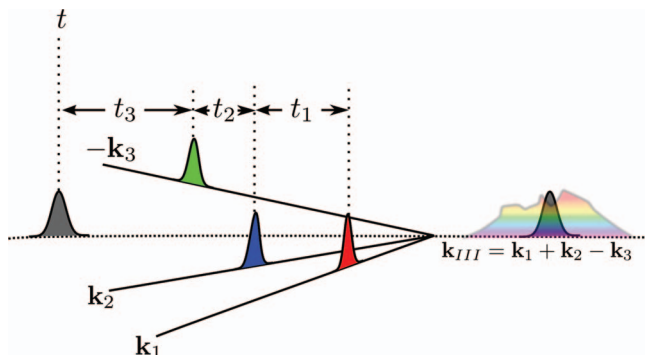


FIG. 2. The XQC technique.

V. COMPUTATIONAL DETAILS

The optimized geometry of formamide was taken from Ref. 39. XCH calculations were performed by converging the electron configuration with a designated core hole and an excited electron on the lowest unoccupied molecular orbital (LUMO). REW-TDDFT calculations were performed with the Tamm-Dancoff approximation. The calculation of DCESs was described in Sec. III B. First a set of XCH-relaxed orbitals are acquired, and the REW-TDDFT equations are solved on this basis. Transition dipole matrix elements between singly and doubly excited states are evaluated between Kohn-Sham determinants with nonorthogonal orbitals using Eq. (10) from Ref. 33:

$$\langle \Psi_A | \hat{d} | \Psi_B \rangle = \sum_{m,n}^{N_{\text{config.}}} a_m b_n \sum_{i,j} (-1)^{i+j} d_{ij}^{mn} \text{Minor}(\mathbf{S}^{mn})_{i,j}, \quad (9)$$

where $\Psi_{A,B}$ are the SCES and DCES wavefunction, respectively, \hat{d} is the transition dipole operator, a_m and b_n are configuration interaction (CI) coefficients for different excited configurations (m and n) of the SCES A and DCES B,

respectively,

$$d_{ij}^{mn} = \sum_{p,q} c_{ip,m,A}^* c_{jq,n,B} \int \phi_p^* \hat{d} \phi_q d\mathbf{r} \quad (10)$$

is the transition dipole matrix between single excitation configurations m and n , $c_{ip,m,A}$ and $c_{jq,n,B}$ are MO coefficients for the configurations m and n of the SCES and DCES, respectively,

$$S_{ij}^{mn} = \sum_{k,l} c_{ik,m,A}^* c_{jl,n,B} \int \phi_i^* \phi_j d\mathbf{r} \quad (11)$$

is the overlap matrix between the MOs of the configurations m and n of state A and B, $\phi_{i,j}$ in Eqs. (10) and (11) are basis functions and i, j, p, q, k, l are indices for these basis functions. $\text{Minor}(\mathbf{S}^{mn})_{i,j}$ denotes the (i, j) minor of the matrix \mathbf{S}^{mn} . All calculations were carried out at the B3LYP^{129,130}/cc-pVTZ¹³¹ level using a modified version of the quantum chemistry package NWChem.^{32,132}

VI. SIMULATION RESULTS

A. XANES

The SCES frequencies (ϵ_e) and transition dipoles (μ_{eg}) were obtained using the REW-TDDFT response approach and a ground state reference wavefunction as described in Sec. II. γ_e , the lifetime broadening of the core-excited state $|e\rangle$, is set to 0.1 eV. The XANES signal

$$S_{\text{XANES}}(\omega) = \frac{1}{\pi} \sum_e \frac{\gamma_e |\mu_{eg}|^2}{(\omega - \epsilon_e)^2 + \gamma_e^2} \quad (12)$$

is shown in Fig. 4. X-ray and electron scattering in the core energy range are known to resemble each other in the gas phase.¹³³ The experimental electron energy loss spectra (EELS) are shown for comparison.

The two lowest-frequency peaks in the experimental nitrogen K-edge EELS are split by 0.95 eV, and the low-

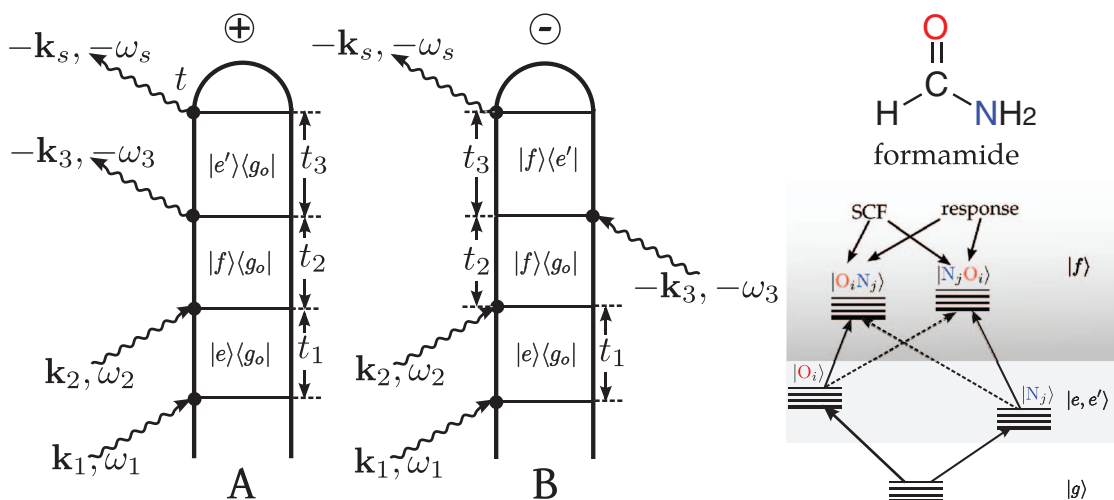


FIG. 3. (Left) The two diagrams contributing to the double quantum coherence signal. (Right) Molecular structure and REW-TDDFT level scheme. $|O_j N_i\rangle$ refers to the double core-excited states with the O1s electron excited to the j th virtual orbital of the self-consistent core state, while the N1s to i th orbital excitation is obtained through response theory, as described in the text.

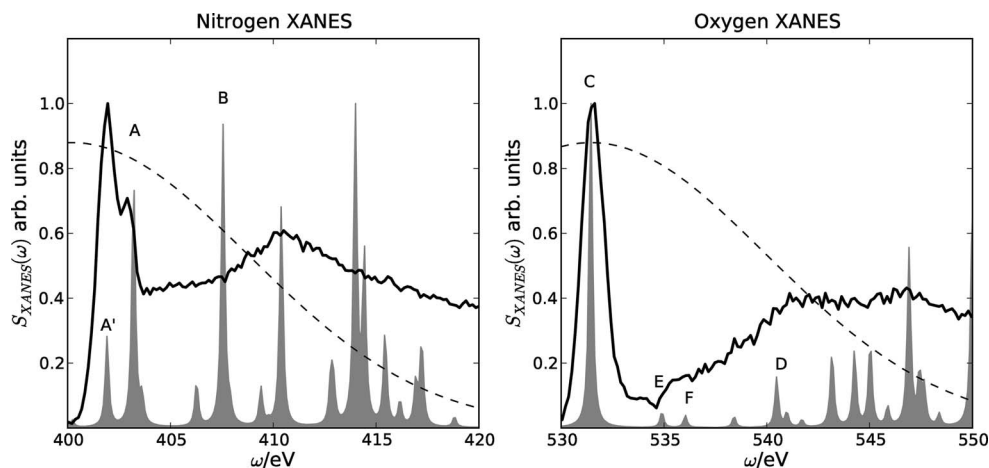


FIG. 4. Calculated (grey) nitrogen (left) and oxygen (right) K-edge XANES for formamide. Experimental EELS spectra¹³⁷ are given as black lines, and power spectra of the pulses used in the calculation of the 2D-QCS signals as dashed lines. The simulated energies were shifted (+13.065 eV for nitrogen and +14.5 eV for oxygen K-edge) to fit the EELS signals.¹³⁷

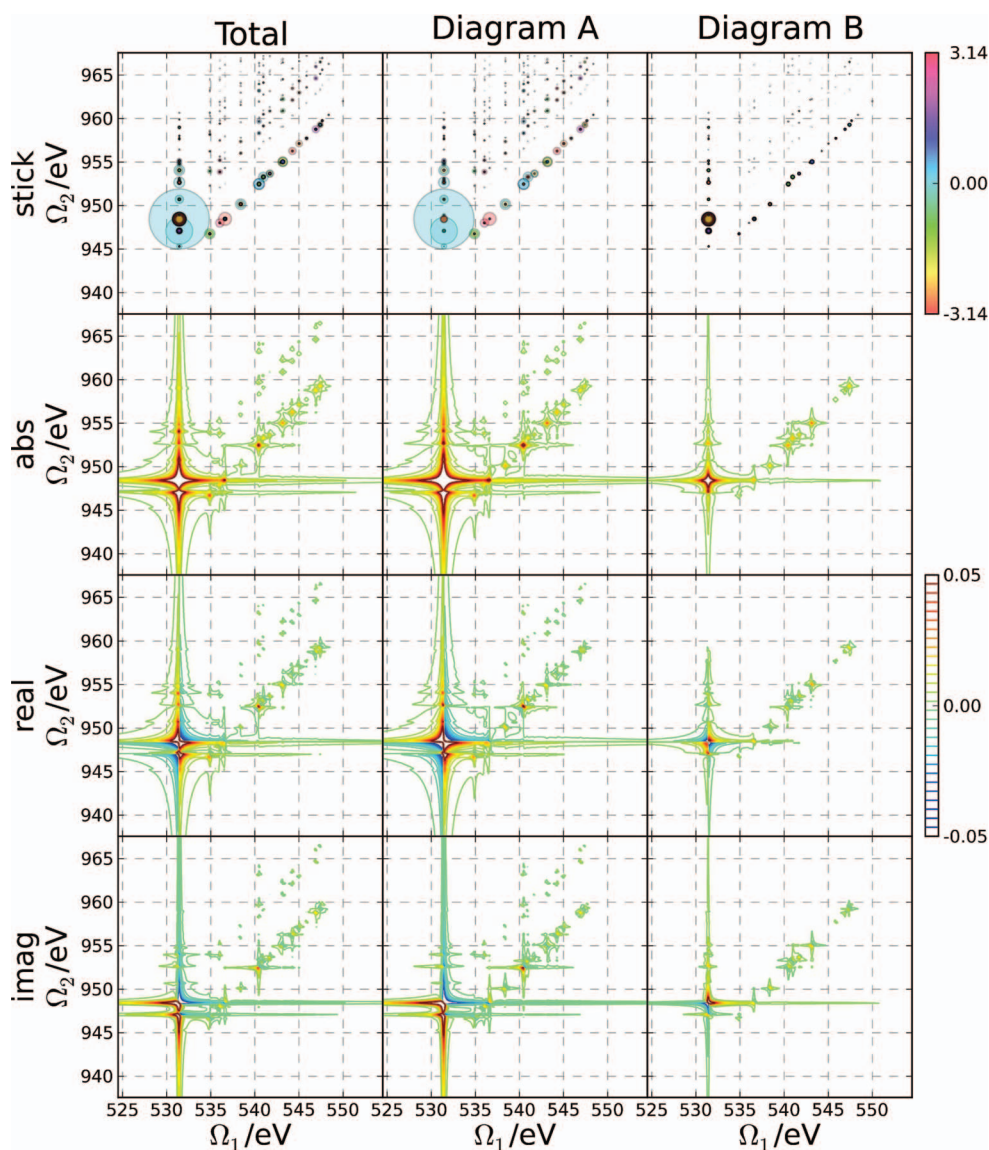


FIG. 5. The $S_{\text{III}}(t_3 = 5 \text{ fs}, \Omega_2, \Omega_1)$ ONNO signal with XXXX polarization configuration. The total signal (left column) is the sum of the contributions from diagram A (middle column) and diagram B (right column) of Fig. 3. Each circle in the stick spectra (top row) has a complex contribution to the signal from a combination of states, with the radius of the circle proportional to the square root of the amplitude, and colored according to the phase of the contributing peak. The following three rows show the absolute value, real and imaginary parts of the complex signal after convoluting with a Lorentzian of width 0.1 eV. All signals were scaled so that $\text{abs}(S_{\text{III}}^{\text{tot}}(t_3 = 5 \text{ fs}, \Omega_2, \Omega_1))$ has a maximum value of one.

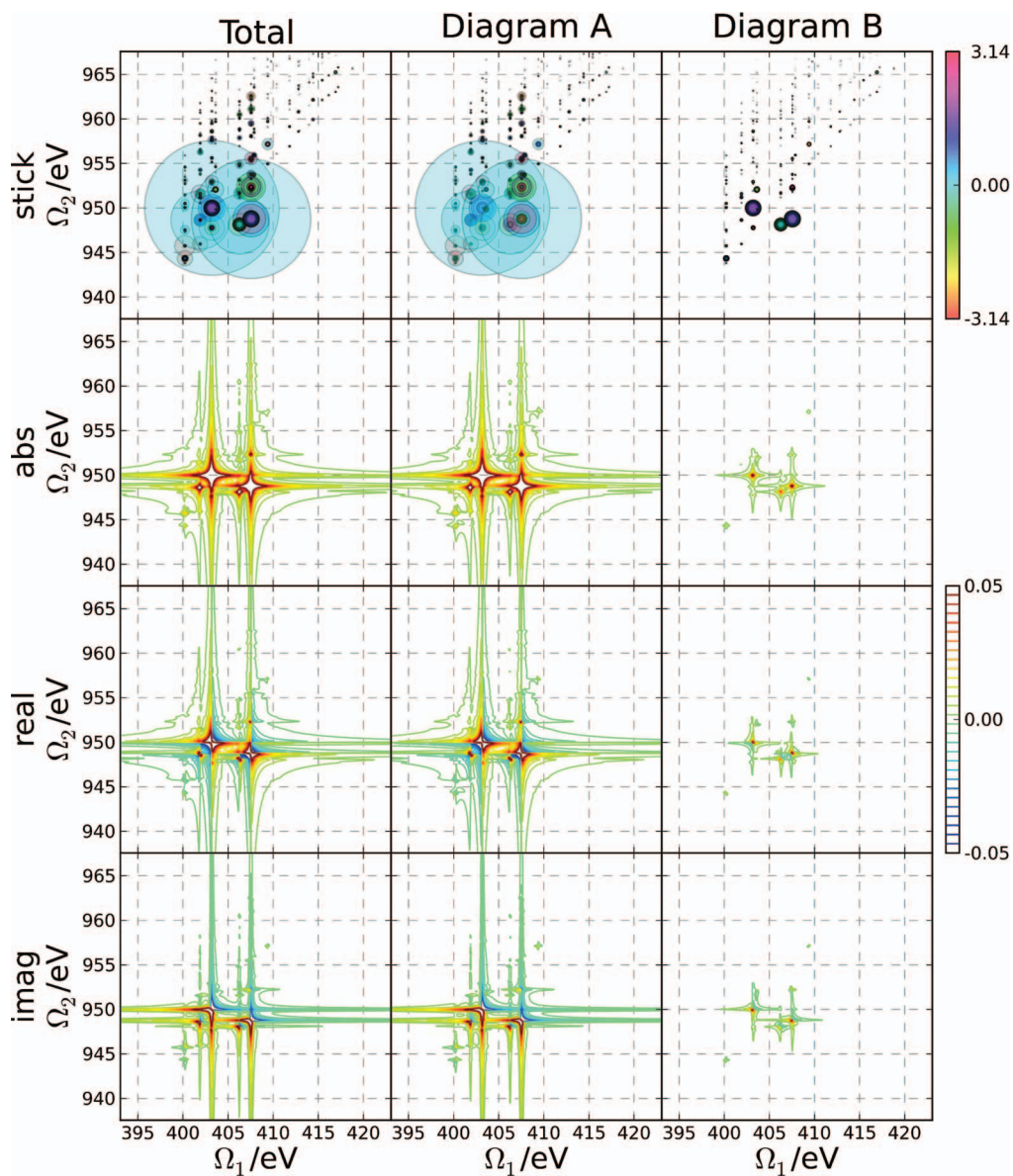
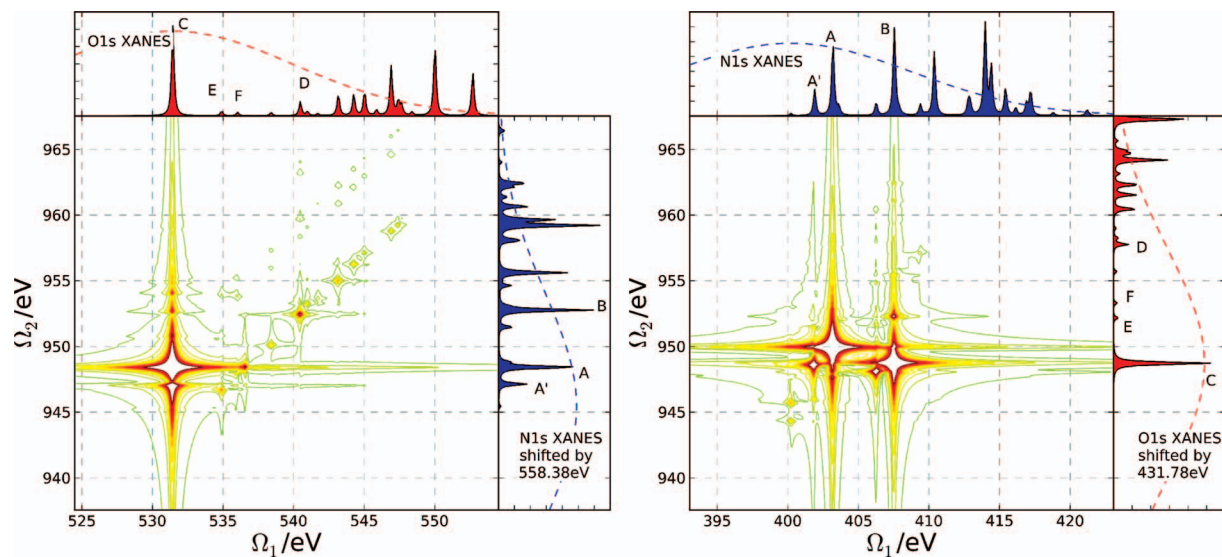


FIG. 6. Same as Fig. 5, but for the pulse sequence NONO.

FIG. 7. Comparison of the absolute parts of the ONNO (left) and NONO (right) $S_{III}(t_3 = 5 \text{ fs}, \Omega_2, \Omega_1)$ signals. XANES spectra are shown in the margins.

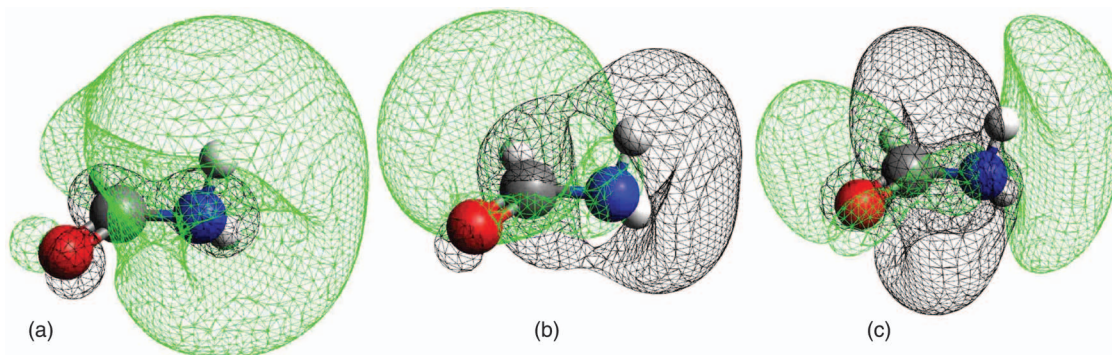


FIG. 8. Dominant MOs of single particle orbitals of different SCEs discussed in Sec. VI B. (a) For peak E and A'. (b) For peak F (c) For peak D. Peaks are labeled in Fig. 4.

energy red peak has an intensity $\times 0.708$ relative to that of the blue peak. Our REW-TDDFT XANES simulations show a larger, 1.29 eV splitting, and a more intense blue component ($\times 2.82$ of the red peak). The simulated oxygen edge

spectrum is much closer to experiment, and the splitting between the lowest-energy peak and higher-energy transitions is reproduced. We see a strong, intense core edge distinct from the higher energy shoulder. Experimental peaks significantly

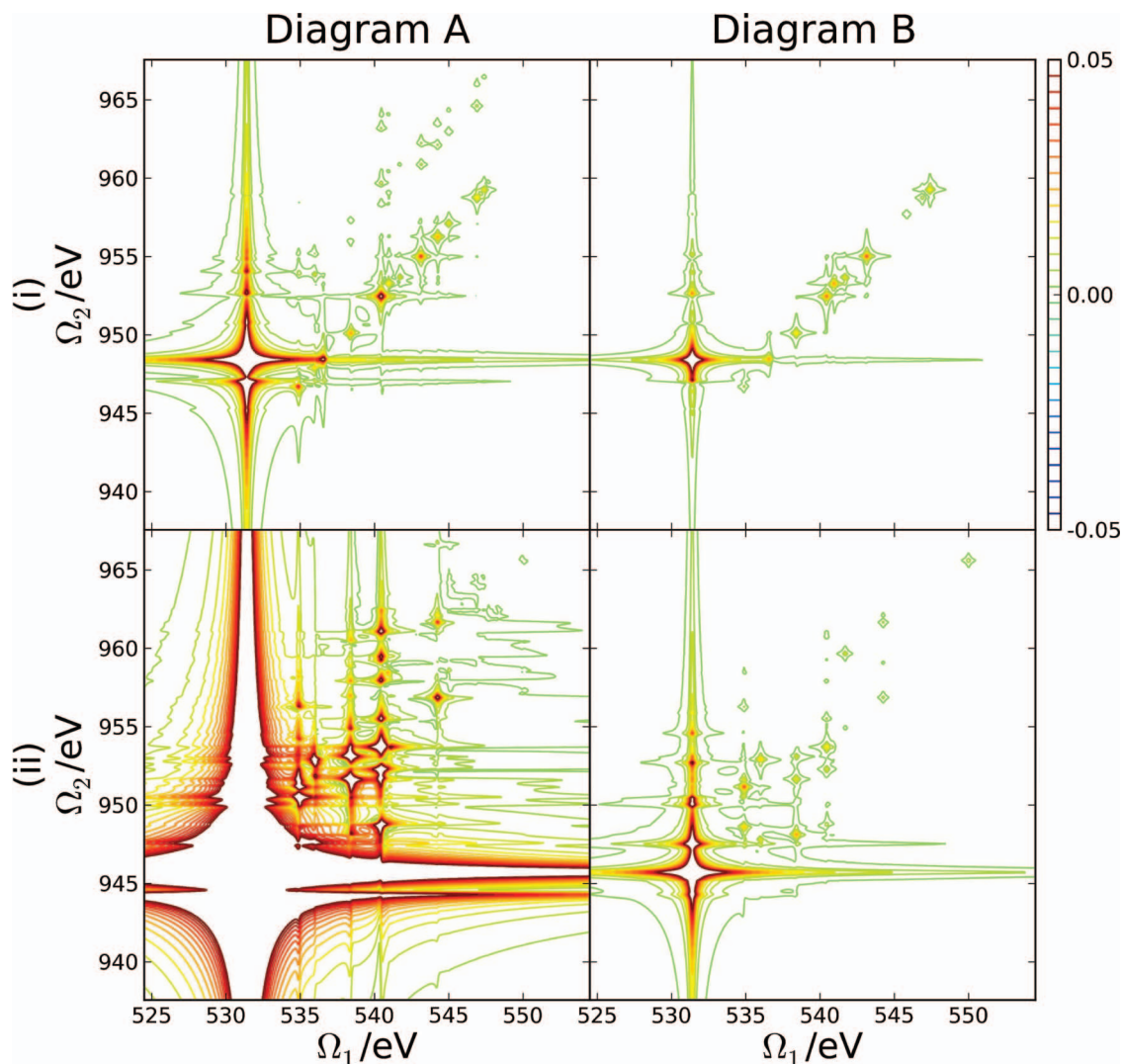


FIG. 9. Comparison of the two protocols to calculate the double-core excited states $|f\rangle$ for the all-parallel ONNO $S_{III}(\ell_3 = 5 \text{ fs}, \Omega_2, \Omega_1)$ signal as discussed in Sec. VI B. Contributions from diagram A (left column) and B (right column) with protocols i (top row) or protocol ii (bottom row). All graphs were multiplied by the same scaling factor used in Fig. 5.

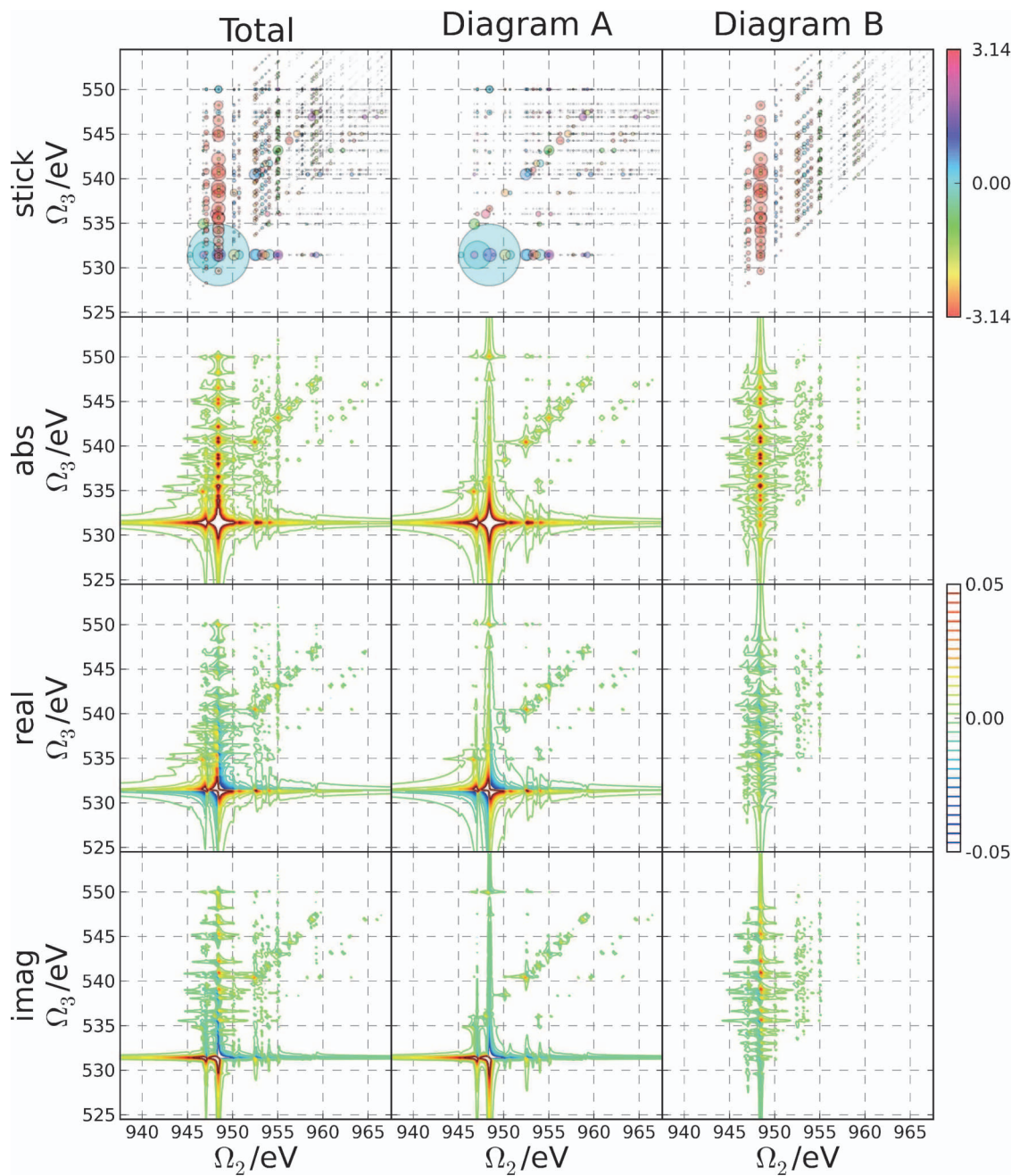


FIG. 10. $S_{\text{III}}(\Omega_3, \Omega_2, t_1 = 5 \text{ fs})$ for the ONNO pulse configuration.

higher than the ionization energy are broadened by coupling to unbound photoelectron states, a process not included in our simulations.

B. The XDQC signal

The $S_{\text{III}}(t_3 = 5 \text{ fs}, \Omega_2, \Omega_1)$ signal is displayed in Figs. 5 and 6. In this plot, resonances on the Ω_1 axis reveal SCES (ω_{eg}), and along the Ω_2 axis we see the DCES (ω_{fg}) frequencies. Time-evolution during the t_3 period results in a phase depending on the final state $|e'\rangle$; these phases are displayed using the colors for each peak in the 2D stick spectrum in the top row.

In Fig. 5, we excite the oxygen core electron first, creating resonances along Ω_1 , and monitor their influence on the nitrogen core excitations, in the DCESs along the Ω_2 axis. This pulse order is marked ONNO. In the NONO spectra shown in Fig. 6 where nitrogen core excitation is first, we see the influence of nitrogen core excitations on the oxygen core excitations. The ONNO signal has resonances in Ω_1 and Ω_3 representing core excitation with the same element, oxygen, in both diagram A ($\Omega_3 \sim \omega_{e'g}$), and diagram B ($\Omega_3 \sim \omega_{fe'}$). Figure 5 shows a typical pattern of the XDQC signal, a series of features lying on parallel lines of roughly constant $\Omega_2 - \Omega_1$ (diagonal character). This pattern indicates weak correlation between the DCESs and SCESs: the energies of the DCESs are roughly the sum of the energies of two SCESs. The

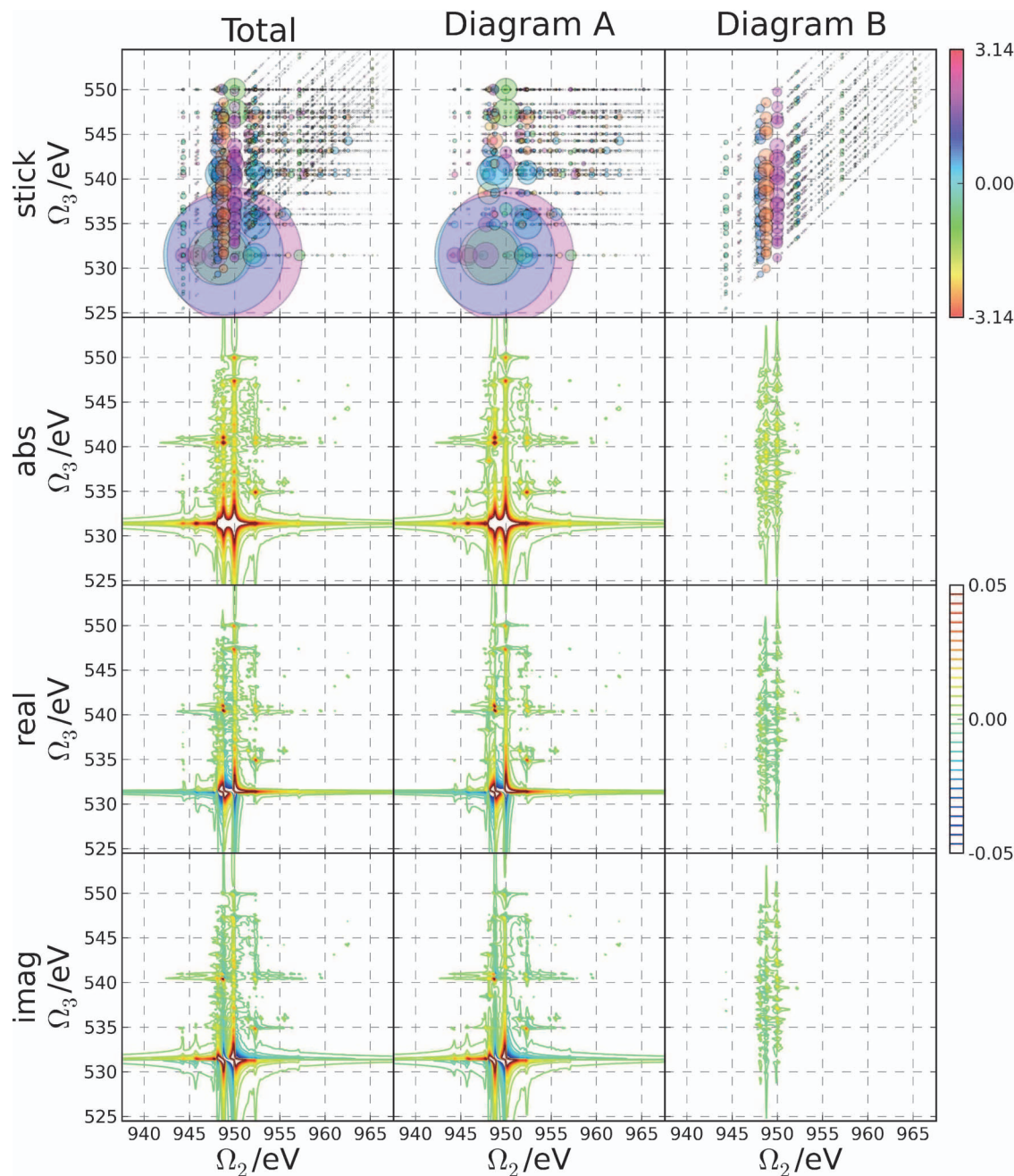


FIG. 11. $S_{\text{III}}(\Omega_3, \Omega_2, t_1 = 5 \text{ fs})$ for the NONO pulse configuration.

oxygen core excitations do not substantially affect the nitrogen core-excitation spectra. In contrast, the NONO signal (Fig. 6) shows a more complicated variation with Ω_1 , in which the diagonal pattern is blurred. Two $|e\rangle$ resonances lie below the diagonal at $\Omega_1 \simeq 407 \text{ eV}$, suggesting that self-consistent relaxation in the field of the nitrogen core hole after the first pulse leads to a set of DCEs during t_2 in which the oxygen and nitrogen excited states strongly interfere. To more closely examine the difference between these two pulse orders, we compare the peak splittings between the XANES and 2D spectra. The energy difference between A' and A is around 1.29 eV in XANES. A' and A correspond to the two strong features in Fig. 5 (shown more clearly in the left panel of Fig. 7), whose energy difference is 1.34 eV, indicating that

the oxygen core hole does not appreciably affect the accessible virtual orbitals during nitrogen single core excitation. However, the energy difference of the two strong features on the Ω_2 axis in Fig. 6 (shown more clearly in the right panel of Fig. 7), shows that the dominant strong oxygen single core excitation is shifted differently by the various nitrogen single core excitations. Comparison of the XDQC to the XANES spectra provides useful insights on correlations between specific core excitations.

To better illustrate the relationship between the 2D-XDQC signal and the linear absorption, we display the ONNO and NONO signals with the XANES marginals in Fig. 7. We shift the N1s and O1s XANES on the Ω_2 axis to match the strongest features. If the core excitations were

uncoupled, the peaks in Ω_2 for a fixed Ω_1 should reproduce the XANES of the core resonant with the second pulse, with one peak quenched due to Pauli repulsion with the previously excited core electron. This might explain the strong diagonal character of the ONNO signal, in which the strong peak A is repeated for increasing Ω_1 . This interpretation does not hold for the NONO signal, with its group of four strong peaks around $\Omega_1 = 405$ eV and $\Omega_2 = 950$ eV. The pattern does not match a shifted XANES signal, implying strong correlations in the DCESs. Comparing the linear absorption (Fig. 4) to the ONNO XDQC signal for $t_3 = 5$ fs (Fig. 5), we find one medium and two stronger features in the nitrogen K-edge XANES, and one strong, two weak and one medium intense features for oxygen K-edge XANES. The corresponding peaks are marked as A', A, B, C, E, F, D in Fig. 4. The N and O K-edge XANES are well described by a single particle picture. The dominant particle MOs in the CI expansions of these SCESs are shown on Fig. 8.

In the ideal zero-DCES-SCES correlation case we expect to see two parallel lines of strong features in Fig. 5 corresponding to A and B in the nitrogen XANES, but we only see one clear set of "diagonal" resonances. The peaks corresponding to states E and F in the oxygen XANES are much weaker than that of D, but their corresponding peaks in the XDQC spectra (in Fig. 5) are as strong as that of D. State E shares the same particle MO as that of A', implying a strong coupling between E and A', which explains the corresponding strong XDQC signal. But for the XDQC peak corresponding to F, it is very difficult to compare the coupling strength of F and A' to that of D and A', simply by their dominant particle MOs. Even the calculated energy of the DCES is close to the sum of two single excitations, the wavefunction is not the simple outer product of two SCES wavefunctions. The single particle picture cannot explain why the XDQC peak corresponding to F also becomes strong, suggesting that many-body effects dominate the signal.

As discussed in Sec. II, the DCES ($|f\rangle$) strongly depend on the order of core excitation by the first two pulses, showing that XDQC is sensitive to the order of the formation of doubly core-excited states. Our XDQC simulations also show large differences between the two protocols explained in the following, reflecting the approximate treatment of many-body effects. In Figs. 5 and 6 we assumed the $|f\rangle$ states were relaxed in the field of the first (core hole a), and calculated using response theory with respect to the second excited core (core hole b, protocol i). In Fig. 9 we present an example of the opposite protocol for the ONNO technique: the $|f\rangle$ states are generated using SCF relaxation for core hole b and then response theory for core hole a (protocol ii). We observe a different blurred line pattern in the spectra obtained with protocol ii (see Fig. 9). Different levels of theory show a different type of DCES-SCES correlation. The protocol i diagram A signal also shows a stronger diagonal component than the corresponding protocol ii signal, which displays a different density of two-particle states on the Ω_2 axis. Comparing XDQC signals from different pulse orders with experiments should reveal how well those theories treat the very specific correlation between a DCES and SCES. This could be valuable in future methodology development for DCESs.

Another portion of the signal, $S_{\text{III}}(\Omega_3, \Omega_2, t_1 = 5 \text{ fs})$, is shown in Figs. 10 and 11. In these graphs, resonances along Ω_2 correspond to doubly excited states (ω_{fg}), and Ω_3 shows the final single excited states ($\omega_{e'g}$ and $\omega_{fe'}$) in the XDQC process. As with the $S_{\text{III}}(t_3 = 5 \text{ fs}, \Omega_2, \Omega_1)$ signals, there are diagonal characteristics in the ONNO spectra (Fig. 10) which are absent in the NONO spectra (Fig. 11). This is a further evidence for the increased correlations for the states probed by the ONNO process. In the $S_{\text{III}}(t_3 = 5 \text{ fs}, \Omega_2, \Omega_1)$ signal the resonances for both A and B diagrams are the same, only the phases for two contributions differ. The $S_{\text{III}}(\Omega_3, \Omega_2, t_1 = 5 \text{ fs})$ signal has qualitatively different peaks along Ω_3 for the two diagrams, as expected, since these diagrams differ in this time period.

VII. CONCLUSIONS

Typically the overlaps of valence holes or electron orbitals are higher than those of core holes or electrons. The correlations between valence excitations are stronger than those between core excitations, which makes the corresponding DQC signals more complicated than those in the present work.¹³⁴ We have demonstrated qualitative differences in the stimulated XDQC signals depending on the order of core excitations at different elements in a small organic molecule. As an experimental technique, XDQC may be used to fingerprint different theoretical approaches for modeling core excitation, by dissecting dynamical doubly-core-excited resonances corresponding to the effects of valence relaxation induced by the core hole. Additional work will be required to further analyze the spectra reported here. First, a detailed description of the valence dynamics, and a comparison of the TDDFT theory with the more easily interpreted orbital theory should highlight the effect of electron correlation on the XDQC signal. Second, with a higher level of theory to describe DCESs, the variation of the Ω_2 resonances with t_1 can be used to measure how the order of core excitation affects the two-particle density of states. The core hole has a unit charge which creates a very strong field over atomic length scales. If the delay between the first two pulses is varied, the changes in the $|f\rangle$ resonances along Ω_2 will reflect the order of perturbation theory necessary to correctly model this strong interaction with the valence band. For short t_1 , linear response theory alone, or supplemented with a full or partial core-hole orbital transformation may adequately capture this effect, as it does in linear absorption. We demonstrated significant differences between the XDQC signals predicted by the calculation protocols. Interpolation between the extremes of linear response (first order), and a full SCF calculation will require a higher level of theory to describe many-body effects in the core excitation.

In the simulations presented here the relaxation of single and double core-excited states, is treated phenomenologically. We only include population decay through Auger or a radiative process that destroys the core hole. We further use the same decay rate for all SCESs and DCESs, independent of the orbitals involved. Interaction of the system with a bath, composed of vibrational and valence-electron degrees of freedom, could introduce additional pure dephasing. Nonlinear spectroscopy has been successful in lower frequency regimes

(NMR to the visible) at disentangling different underlying mechanisms for excited-state decay and dephasing.¹³⁵ Similar effects are expected in core-excitation spectra. Estimating their magnitude, comparing them to population decay rates, and designing experiments that distinguish between them is an interesting future topic. One manifestation of these effects in existing X-ray experiments are fluorescence vs. Raman signals, which are controlled by the ratio of pure dephasing and population relaxation rates.

ACKNOWLEDGMENTS

We gratefully acknowledge the support of the Chemical Sciences, Geosciences and Biosciences Division, Office of Basic Energy Sciences, Office of Science, U.S. Department of Energy, the support of the National Science Foundation (NSF) through Grant No. CHE-1058791 and the National Institute of Health (Grant No. GM-59230). Help on the REW-TDDFT calculations from Niranjana Govind of the Pacific Northwest National Lab (PNNL) is greatly appreciated.

APPENDIX: ORIENTATIONAL TENSOR AVERAGING

The dipole and electric field polarization tensor contributions to the signal must be rotationally averaged over all possible orientations of the molecule. The rotationally averaged¹³⁶ signal is

$$S_{\text{III}}^{\text{rot}} = \frac{1}{30} \begin{pmatrix} S_{\text{III}}^{\alpha} \\ S_{\text{III}}^{\beta} \\ S_{\text{III}}^{\gamma} \end{pmatrix} \begin{pmatrix} 4 & -1 & -1 \\ -1 & 4 & -1 \\ -1 & -1 & 4 \end{pmatrix} \begin{pmatrix} \cos \theta_{12} \cos \theta_{34} \\ \cos \theta_{13} \cos \theta_{24} \\ \cos \theta_{14} \cos \theta_{23} \end{pmatrix}, \quad (\text{A1})$$

where $\cos \theta_{ij} = \hat{e}_i \cdot \hat{e}_j$, \hat{e}_i is the polarization of the i th pulse polarization vector, and $S_{\alpha, \beta, \gamma}$ represent various contractions over the tensor components of the response,

$$S_{\text{III}}^{\alpha} = \sum_{\nu_1 \nu_2} S_{\text{III}}^{\nu_2 \nu_2 \nu_1 \nu_1}, \quad (\text{A2})$$

$$S_{\text{III}}^{\beta} = \sum_{\nu_1 \nu_2} S_{\text{III}}^{\nu_2 \nu_1 \nu_2 \nu_1}, \quad (\text{A3})$$

and

$$S_{\text{III}}^{\gamma} = \sum_{\nu_1 \nu_2} S_{\text{III}}^{\nu_1 \nu_2 \nu_2 \nu_1}. \quad (\text{A4})$$

For the all parallel pulse configuration, the signal is proportional to the sum of all three

$$S_{\text{III}}^{\text{rot}} = \frac{1}{15} (S_{\text{III}}^{\alpha} + S_{\text{III}}^{\beta} + S_{\text{III}}^{\gamma}). \quad (\text{A5})$$

¹T. Popmintchev, M.-C. Chen, P. Arpin, M. M. Murnane, and H. C. Kapteyn, *Nat. Photonics* **4**, 822 (2010).

²F. Krausz and M. Ivanov, *Rev. Mod. Phys.* **81**, 163 (2009).

³P. Emma, R. Akre, J. Arthur, R. Bionta, C. Bostedt, J. Bozek, A. Brachmann, P. Bucksbaum, R. Coffee, F.-J. Decker, Y. Ding, D. Dowell, S. Edstrom, A. Fisher, J. Frisch, S. Gilevich, J. Hastings, G. Hays, P. Hering, Z. Huang, R. Iverson, H. Loos, M. Messerschmidt, A. Miahnahri, S. Moeller, H.-D. Nuhn, G. Pile, D. Ratner, J. Rzepiela, D. Schultz, T.

Smith, P. Stefan, H. Tompkins, J. Turner, J. Welch, W. White, J. Wu, G. Yocky, and J. Galayda, *Nat. Photonics* **4**, 641 (2010).

⁴J. Ullrich, A. Rudenko, and R. Moshhammer, *Annu. Rev. Phys. Chem.* **63**, 635 (2012).

⁵L. Young, E. P. Kanter, B. Krässig, Y. Li, A. M. March, S. T. Pratt, R. Santra, S. H. Southworth, N. Rohringer, L. F. DiMauro, G. Doumy, C. A. Roedig, N. Berrah, L. Fang, M. Hoener, P. H. Bucksbaum, J. P. Cryan, S. Ghimire, J. M. Glowia, D. A. Reis, J. D. Bozek, C. Bostedt, and M. Messerschmidt, *Nature (London)* **466**, 56 (2010).

⁶M. Hoener, L. Fang, O. Kornilov, O. Gessner, S. T. Pratt, M. Gühr, E. P. Kanter, C. Blaga, C. Bostedt, J. D. Bozek, P. H. Bucksbaum, C. Buth, M. Chen, R. Coffee, J. Cryan, L. DiMauro, M. Glowia, E. Hosler, E. Kukk, S. R. Leone, B. McFarland, M. Messerschmidt, B. Murphy, V. Petrovic, D. Rolles, and N. Berrah, *Phys. Rev. Lett.* **104**, 253002 (2010).

⁷P. Elliott, S. Goldson, C. Canahui, and N. T. Maitra, *Chem. Phys.* **391**, 110 (2011).

⁸J.-P. Connerade, *Highly Excited Atoms* (Cambridge University Press, 1998).

⁹R. Santra, N. V. Kryzhevoi, and L. S. Cederbaum, *Phys. Rev. Lett.* **103**, 013002 (2009).

¹⁰K. Ueda and O. Takahashi, *J. Electron Spectrosc. Relat. Phenom.* **185**, 301 (2012).

¹¹N. V. Kryzhevoi, R. Santra, and L. S. Cederbaum, *J. Chem. Phys.* **135**, 084302 (2011).

¹²P. Salén, P. van der Meulen, H. T. Schmidt, R. D. Thomas, M. Larsson, R. Feifel, M. N. Piancastelli, L. Fang, B. Murphy, T. Osipov, N. Berrah, E. Kukk, K. Ueda, J. D. Bozek, C. Bostedt, S. Wada, R. Richter, V. Feyer, and K. C. Prince, *Phys. Rev. Lett.* **108**, 153003 (2012).

¹³M. Tashiro, K. Ueda, and M. Ehara, *Chem. Phys. Lett.* **521**, 45 (2012).

¹⁴J. Kim, S. Mukamel, and G. D. Scholes, *Acc. Chem. Res.* **42**, 1375 (2009).

¹⁵S. Mukamel, R. Oszwaldowski, and D. Abramavicius, *Phys. Rev. B* **75**, 245305 (2007).

¹⁶W. Zhuang, D. Abramavicius, and S. Mukamel, *Proc. Natl. Acad. Sci. U.S.A.* **102**, 7443 (2005).

¹⁷A. Nemeth, F. Milota, T. Mančal, T. Pullerits, J. Sperling, J. Hauer, H. F. Kauffmann, and N. Christensson, *J. Chem. Phys.* **133**, 094505 (2010).

¹⁸S. Mukamel, R. Oszwaldowski, and L. Yang, *J. Chem. Phys.* **127**, 221105 (2007).

¹⁹D. Karaiskaj, A. D. Bristow, L. Yang, X. Dai, R. P. Mirin, S. Mukamel, and S. T. Cundiff, *Phys. Rev. Lett.* **104**, 117401 (2010).

²⁰K. W. Stone, K. Gundogdu, D. B. Turner, X. Li, S. T. Cundiff, and K. A. Nelson, *Science* **324**, 1169 (2009).

²¹X. Dai, M. Richter, H. Li, A. D. Bristow, C. Falvo, S. Mukamel, and S. T. Cundiff, *Phys. Rev. Lett.* **108**, 193201 (2012).

²²J. Orenstein, *Phys. Today* **65**(9), 44 (2012).

²³G. D. Mahan, *Condensed Matter in a Nutshell* (Princeton University Press, 2011).

²⁴D. Fausti, R. I. Tobey, N. Dean, S. Kaiser, A. Dienst, M. C. Hoffmann, S. Pyon, T. Takayama, H. Takagi, and A. Cavalleri, *Science* **331**, 189 (2011).

²⁵I. V. Schweigert and S. Mukamel, *Phys. Rev. A* **78**, 052509 (2008).

²⁶M. Stener, G. Fronzoni, and M. de Simone, *Chem. Phys. Lett.* **373**, 115 (2003).

²⁷N. A. Besley and A. Noble, *J. Phys. Chem. C* **111**, 3333 (2007).

²⁸S. DeBeer-George, T. Petrenko, and F. Neese, *J. Phys. Chem. A* **112**, 12936 (2008).

²⁹N. A. Besley, M. J. G. Peach, and D. J. Tozer, *Phys. Chem. Chem. Phys.* **11**, 10350 (2009).

³⁰N. A. Besley and F. A. Asmuruf, *Phys. Chem. Chem. Phys.* **12**, 12024 (2010).

³¹W. Liang, S. A. Fischer, M. J. Frisch, and X. Li, *J. Chem. Theory Comput.* **7**, 3540 (2011).

³²K. Lopata, B. E. V. Kuiken, M. Khalil, and N. Govind, *J. Chem. Theory Comput.* **8**, 3284 (2012).

³³Y. Zhang, J. D. Biggs, D. Healion, N. Govind, and S. Mukamel, *J. Chem. Phys.* **137**, 194306 (2012).

³⁴N. Ottosson, E. F. Aziz, H. Bergersen, W. Pokapanich, G. Öhrwall, S. Svensson, W. Eberhardt, and O. Björneholm, *J. Phys. Chem. B* **112**, 16642 (2008).

³⁵N. Ottosson, E. F. Aziz, I. L. Bradeanu, S. Legendre, G. Öhrwall, S. Svensson, O. Björneholm, and W. Eberhardt, *Chem. Phys. Lett.* **460**, 540 (2008).

³⁶H. Ikeura-Sekiguchi, T. Sekiguchi, Y. Kitajima, and Y. Baba, *Appl. Surf. Sci.* **169-170**, 282 (2001).

³⁷D. P. Chong, *J. Electron Spectrosc. Relat. Phenom.* **184**, 164 (2011).

- ³⁸H. Ågren and H. J. A. Jensen, *Chem. Phys.* **172**, 45 (1993).
- ³⁹O. Takahashi, M. Tashiro, M. Ehara, K. Yamasaki, and K. Ueda, *Chem. Phys.* **384**, 28 (2011).
- ⁴⁰J. Jadczyk and J. Świergiel, *Phys. Chem. Chem. Phys.* **14**, 3170 (2012).
- ⁴¹Y. L. Li, L. Huang, R. J. D. Miller, T. Hasegawa, and Y. Tanimura, *J. Chem. Phys.* **128**, 234507 (2008).
- ⁴²A. Paarmann, M. Lima, R. Chelli, V. V. Volkov, R. Righini, and R. J. D. Miller, *Phys. Chem. Chem. Phys.* **13**, 11351 (2011).
- ⁴³J. Jortner and S. A. Rice, *J. Chem. Phys.* **44**, 3364 (1966).
- ⁴⁴D. Sangalli, P. Romaniello, G. Onida, and A. Marini, *J. Chem. Phys.* **134**, 034115 (2011).
- ⁴⁵L. Serrano-Andres, M. Merchán, I. Nebot-Gil, R. Lindh, and B. O. Roos, *J. Chem. Phys.* **98**, 3151 (1993).
- ⁴⁶K. Nakayama, H. Nakano, and K. Hirao, *Int. J. Quantum Chem.* **66**, 157 (1998).
- ⁴⁷C. Hsu, S. Hirata, and M. Head-Gordon, *J. Phys. Chem. A* **105**, 451 (2001).
- ⁴⁸J. H. Starcke, M. Wormit, J. Schirmer, and A. Dreuw, *Chem. Phys.* **329**, 39 (2006).
- ⁴⁹J. H. Starcke, M. Wormit, and A. Dreuw, *J. Chem. Phys.* **131**, 144311 (2009).
- ⁵⁰S. Knippenberg, J. H. Starcke, M. Wormit, and A. Dreuw, *Mol. Phys.* **108**, 2801 (2010).
- ⁵¹C. Angeli and M. Pastore, *J. Chem. Phys.* **134**, 184302 (2011).
- ⁵²M. Schmidt and P. Tavan, *J. Chem. Phys.* **136**, 124309 (2012).
- ⁵³E. Otero, N. Kosugi, and S. G. Uguhart, *J. Chem. Phys.* **131**, 114313 (2009).
- ⁵⁴M. E. Casida, *J. Chem. Phys.* **122**, 054111 (2005).
- ⁵⁵M. Casida, A. Ipatov, and F. Cordova, in *Time-Dependent Density Functional Theory*, Lecture Notes in Physics Vol. 706, edited by M. A. Marques, C. A. Ullrich, F. Nogueira, A. Rubio, K. Burke, and E. K. U. Gross (Springer-Verlag, Berlin, 2006), Chap. 16, p. 243.
- ⁵⁶P. Th. van Duijnen, S. N. Greene, and N. G. J. Richards, *J. Chem. Phys.* **127**, 045105 (2007).
- ⁵⁷Z. Li and W. Liu, *J. Chem. Phys.* **133**, 064106 (2010).
- ⁵⁸Y. Kurashige, H. Nakano, Y. Nakao, and K. Hirao, *Chem. Phys. Lett.* **400**, 425 (2004).
- ⁵⁹V. Carravetta, and H. Ågren, in *Computational Strategies for Spectroscopy*, edited by V. Barone (John Wiley & Sons, Inc., 2011), pp. 137–205.
- ⁶⁰O. Lehtonen, D. Sundholm, R. Send, and M. P. Johansson, *J. Chem. Phys.* **131**, 024301 (2009).
- ⁶¹C. M. Marian and N. Gilka, *J. Chem. Theory Comput.* **4**, 1501 (2008).
- ⁶²I. A. Mikhailov, S. Tafur, and A. E. Masunov, *Phys. Rev. A* **77**, 012510 (2008).
- ⁶³*Time-Dependent Density Functional Theory*, edited by M. A. Marques, C. A. Ullrich, F. Nogueira, A. Rubio, K. Burke, and E. K. U. Gross (Springer, 2006).
- ⁶⁴C. A. Ullrich, *Time-Dependent Density Functional Theory: Concepts and Applications* (Oxford University Press, New York, 2012).
- ⁶⁵N. T. Maitra, F. Zhang, R. J. Cave, and K. Burke, *J. Chem. Phys.* **120**, 5932 (2004).
- ⁶⁶S. Tretiak, V. Chernyak, and S. Mukamel, *Int. J. Quantum Chem.* **70**, 711 (1998).
- ⁶⁷S. Tretiak and V. Chernyak, *J. Chem. Phys.* **119**, 8809 (2003).
- ⁶⁸E. K. U. Gross, J. F. Dobson, and M. Petersilka, in *Density-Functional Theory II*, Topics in Current Chemistry Vol. 181, edited by R. F. Nalewajski (Springer, Berlin, 1996), p. 81.
- ⁶⁹S. Hirata and M. Head-Gordon, *Chem. Phys. Lett.* **314**, 291 (1999).
- ⁷⁰R. J. Cave, F. Zhang, N. T. Maitra, and K. Burke, *Chem. Phys. Lett.* **389**, 39 (2004).
- ⁷¹G. Mazur and R. Włodarczyk, *J. Comput. Chem.* **30**, 811 (2009).
- ⁷²G. Mazur, M. Makowski, R. Włodarczyk, and Y. Aoki, *Int. J. Quantum Chem.* **111**, 819 (2011).
- ⁷³M. Huix-Rotllant, A. Ipatov, A. Rubio, and M. E. Casida, *Chem. Phys.* **391**, 120 (2011).
- ⁷⁴P. Romaniello, D. Sangalli, J. A. Berger, F. Sottile, L. G. Molinari, L. Reining, and G. Onida, *J. Chem. Phys.* **130**, 044108 (2009).
- ⁷⁵A. I. Krylov, *Chem. Phys. Lett.* **338**, 375 (2001).
- ⁷⁶A. I. Krylov, *Chem. Phys. Lett.* **350**, 522 (2001).
- ⁷⁷A. I. Krylov and C. D. Sherrill, *J. Chem. Phys.* **116**, 3194 (2002).
- ⁷⁸L. V. Slipchenko and A. I. Krylov, *J. Chem. Phys.* **117**, 4694 (2002).
- ⁷⁹Y. Shao, M. Head-Gordon, and A. I. Krylov, *J. Chem. Phys.* **118**, 4807 (2003).
- ⁸⁰F. Wang and T. Ziegler, *J. Chem. Phys.* **121**, 12191 (2004).
- ⁸¹Z. Rinkevicius, O. Vahtras, and H. Ågren, *J. Chem. Phys.* **133**, 114104 (2010).
- ⁸²N. Minezawa and M. S. Gordon, *J. Phys. Chem. A* **115**, 7901 (2011).
- ⁸³Z. Li and W. Liu, *J. Chem. Phys.* **136**, 024107 (2012).
- ⁸⁴Y. A. Bernard, Y. Shao, and A. I. Krylov, *J. Chem. Phys.* **136**, 204103 (2012).
- ⁸⁵C. M. Isborn and X. Li, *J. Chem. Phys.* **129**, 204107 (2008).
- ⁸⁶W. Liang, C. M. Isborn, and X. Li, *J. Chem. Phys.* **131**, 204101 (2009).
- ⁸⁷V. N. Glushkov and X. Assfeld, *J. Chem. Phys.* **132**, 204106 (2010).
- ⁸⁸V. N. Glushkov and X. Assfeld, *J. Comput. Chem.* **33**, 2058 (2012).
- ⁸⁹K. J. H. Giesbertz, E. J. Baerends, and O. V. Gritsenko, *Phys. Rev. Lett.* **101**, 033004 (2008).
- ⁹⁰P. Nozieres and C. T. D. Dominicis, *Phys. Rev.* **178**, 1097 (1969).
- ⁹¹W. H. E. Schwarz and R. J. Buenker, *Chem. Phys.* **13**, 153 (1976).
- ⁹²I. V. Schweigert and S. Mukamel, *Phys. Rev. Lett.* **99**, 163001 (2007).
- ⁹³I. V. Schweigert and S. Mukamel, *Phys. Rev. A* **76**, 012504 (2007).
- ⁹⁴I. V. Schweigert and S. Mukamel, *J. Chem. Phys.* **128**, 184307 (2008).
- ⁹⁵D. M. Healion, I. V. Schweigert, and S. Mukamel, *J. Phys. Chem. A* **112**, 11449 (2008).
- ⁹⁶M. N. R. Wohlfarth and L. S. Cederbaum, *J. Chem. Phys.* **116**, 8723 (2002).
- ⁹⁷M. Cavalleri, M. Odelius, D. Nordlund, A. Nilsson, and L. G. Pettersson, *Phys. Chem. Chem. Phys.* **7**, 2854 (2005).
- ⁹⁸H. Ågren, V. Carravetta, O. Vahtras, and L. G. M. Pettersson, *Chem. Phys. Lett.* **222**, 75 (1994).
- ⁹⁹H. Ågren, V. Carravetta, O. Vahtras, and L. G. M. Pettersson, *Theor. Chem. Acc.* **97**, 14 (1997).
- ¹⁰⁰W. J. Hunt and W. A. Goddard III, *Chem. Phys. Lett.* **3**, 414 (1969).
- ¹⁰¹D. Healion, H. Wang, and S. Mukamel, *J. Chem. Phys.* **134**, 124101 (2011).
- ¹⁰²J. D. Biggs, Y. Zhang, D. Healion, and S. Mukamel, *J. Chem. Phys.* **136**, 174117 (2012).
- ¹⁰³J. H. D. Eland, M. Tashiro, P. Linusson, M. Ehara, K. Ueda, and R. Feifel, *Phys. Rev. Lett.* **105**, 213005 (2010).
- ¹⁰⁴L. Inhester, C. F. Burmeister, G. Groenhof, and H. Grubmüller, *J. Chem. Phys.* **136**, 144304 (2012).
- ¹⁰⁵J. Schirmer, L. S. Cederbaum, and O. Walter, *Phys. Rev. A* **28**, 1237 (1983).
- ¹⁰⁶J. Schirmer and A. Barth, *Z. Phys. A* **317**, 267 (1984).
- ¹⁰⁷J. Niskanen, P. Norman, H. Aksela, and H. Ågren, *J. Chem. Phys.* **135**, 054310 (2011).
- ¹⁰⁸O. Takahashi, M. Tashiro, M. Ehara, K. Yamasaki, and K. Ueda, *J. Phys. Chem. A* **115**, 12070 (2011).
- ¹⁰⁹O. Takahashi, K. Yamasaki, S. Nagaoka, and K. Ueda, *Chem. Phys. Lett.* **518**, 44 (2011).
- ¹¹⁰A. T. B. Gilbert, N. A. Besley, and P. M. W. Gill, *J. Phys. Chem. A* **112**, 13164 (2008).
- ¹¹¹U. Ekström, P. Norman, V. Carravetta, and H. Ågren, *Phys. Rev. Lett.* **97**, 143001 (2006).
- ¹¹²M. Linares, S. Stafström, Z. Rinkevicius, H. Ågren, and P. Norman, *J. Phys. Chem. B* **115**, 5096 (2011).
- ¹¹³B. Brena, P. E. M. Siegbahn, and H. Ågren, *J. Am. Chem. Soc.* **134**, 17157 (2012).
- ¹¹⁴A. Nardelli, G. Fronzoni, and M. Stener, *Phys. Chem. Chem. Phys.* **13**, 480 (2011).
- ¹¹⁵J. P. Perdew and A. Zunger, *Phys. Rev. B* **23**, 5048 (1981).
- ¹¹⁶G. Tu, Z. Rinkevicius, O. Vahtras, H. Ågren, U. Ekström, P. Norman, and V. Carravetta, *Phys. Rev. A* **76**, 022506 (2007).
- ¹¹⁷A. Nakata, Y. Imamura, T. Ostuka, and H. Nakai, *J. Chem. Phys.* **124**, 094105 (2006).
- ¹¹⁸A. Nakata, Y. Imamura, and H. Nakai, *J. Chem. Phys.* **125**, 064109 (2006).
- ¹¹⁹Y. Imamura, R. Kobayashi, and H. Nakai, *J. Chem. Phys.* **134**, 124113 (2011).
- ¹²⁰J.-W. Song, M. A. Watson, A. Nakata, and K. Hirao, *J. Chem. Phys.* **129**, 184113 (2008).
- ¹²¹D. Prendergast and G. Galli, *Phys. Rev. Lett.* **96**, 215502 (2006).
- ¹²²M. Tailliefumier, D. Cabaret, A.-M. Flank, and F. Mauri, *Phys. Rev. B* **66**, 195107 (2002).
- ¹²³A. Ipatov, F. Cordova, L. J. Doriol, and M. E. Casida, *J. Mol. Struct.: THEOCHEM* **914**, 60 (2009).
- ¹²⁴Z. Li, W. Liu, Y. Zhang, and B. Suo, *J. Chem. Phys.* **134**, 134101 (2011).

- ¹²⁵Z. Li and W. Liu, *J. Chem. Phys.* **135**, 194106 (2011).
- ¹²⁶I. V. Schweigert and S. Mukamel, *Phys. Rev. A* **77**, 033802 (2008).
- ¹²⁷J. D. Biggs, J. A. Voll, and S. Mukamel, *Philos. Trans. R. Soc. London, Ser. A* **370**, 3709 (2012).
- ¹²⁸O. Roslyak, B. Fingerhut, K. Bennett, and S. Mukamel, "Quasiparticle representation of coherent nonlinear optical signals of multiexcitons," *Phys. Rev. B* (submitted).
- ¹²⁹A. D. Becke, *J. Chem. Phys.* **98**, 5648 (1993).
- ¹³⁰P. Stephens, F. Devlin, C. Chabalowski, and M. Frisch, *J. Phys. Chem.* **98**, 11623 (1994).
- ¹³¹T. H. Dunning, *J. Chem. Phys.* **90**, 1007 (1989).
- ¹³²M. Valiev, E. Bylaska, N. Govind, K. Kowalski, T. Straatsma, H. van Dam, D. Wang, J. Nieplocha, E. Apra, T. Windus, and W. de Jong, *Comput. Phys. Commun.* **181**, 1477 (2010).
- ¹³³J. Stöhr, *NEXAFS Spectroscopy* (Springer-Verlag, 1992), pp. 34–39.
- ¹³⁴Z. Li, D. Abramavicius, and S. Mukamel, *J. Am. Chem. Soc.* **130**, 3509 (2008).
- ¹³⁵S. Mukamel, *Principles of Nonlinear Optical Spectroscopy* (Oxford University Press, New York, 1999).
- ¹³⁶D. L. Andrews and T. Thirunamachandran, *J. Chem. Phys.* **67**, 5026 (1977).
- ¹³⁷M. Robin, I. Ishii, R. McLaren, and A. Hitchcock, *J. Electron Spectrosc. Relat. Phenom.* **47**, 53 (1988).